A predictive mechano-biological model of the bone-implant healing

Dominique Ambard, Pascal Swider

Biomechanics Laboratory EA3697/IFR30, University of Toulouse 3, CHU Purpan, Toulouse, France

Abstract

The quality of the fixation orthopaedic implant to its surrounding bone determines its clinical longevity. Up to 20% of hip replacement operations are currently revisions for aseptic loosening. While this fixation quality is determined primarily by the bone and tissue anchoring the implant, conditions influencing bone growth in the early post-operative period include the surgical technique and coupled mechanical and biochemical factors. The aim of the study was to propose an original mechano-biological formulation of the healing process of periprosthetic tissue. The multiphasic porous model involved the solid osseous matrix, the extracellular fluid phase, the osteoblastic cellular phase responsible from the bone formation and the growth factor phase promoting the cellular activity. To derive the non-linear convective-diffuse governing equations, mass balance was associated to cell active haptotactic and chemotactic migration, growth factor diffusion, cell proliferation (logistic law) and bone formation (reactive medium). The in-vivo application concerned a canine axisymmetric implant which was stable and mechanically unloaded. Predictive numerical results were compared to ex-vivo data from a histologic study. The generic healing pattern involving two main oscillations of the radial bone formation was well predicted. In the future, the model could assist in evaluating the role of growth factor concentrations and their temporal delivering as far as the role of pertinent sources such as bioactive coating or additional biomaterials.

Keywords: Biomechanics; Porous media; Diffusion; Convection; Cell migration

1. Introduction

The quality of the fixation of an implant to its surrounding bone determines its clinical longevity. Total hip arthroplasty improves patient quality of life, and at 10–15 years approximately 95% of the implants are still functioning well. However, up to 20% of hip replacement operations currently are revisions for aseptic loosening. While this fixation quality is determined primarily by the bone and tissue anchoring the implant, conditions influencing bone growth in the early post-operative period include the surgical technique and coupled mechanical and biochemical factors (Hahn et al., 1998).

The biological phases of the implant healing process are presented in Fig. 1. The initial bleeding phase last a few hours. The vasodilatation induces plasma and leucocytes supply, as far as macrophage cells which recycle cellular and tissue debris. During the inflammatory phase, concomitant clot involving blood platelet is created and cellular elements synthesize growth factors. Growth factors are proteins responsible for regulating cell pro-

Nomenclature

m^{t}	total mass of macroscopic volume element	kg	
m^{s}	mass of solid phase (osseous matrix) per volume element	kg	
m^{f}	mass of fluid phase (bone marrow) per volume element	kg	
m^{c}	mass of cells (osteoblast) per volume element	kg	
m^{m}	mass of growth factors per volume element	kg	
ρ^{s}	density of solid phase	kg/mm^3	
ρ^{f}	density of fluid phase	kg/mm^3	
v^{t}	total volume of macroscopic element	mm^3	
v^{s}	volume of solid phase per macroscopic element	mm^3	
v^{f}	volume of fluid phase per macroscopic element	mm^3	
N^{c}	number of cells	cell	
N^{M}	amount of growth factors	ng	
n^{c}	amount of cells per macroscopic element	cell/mm^3	
n^{M}	amount of growth factors per macroscopic element	ng/mm^3	
ϕ^{s}	solid fraction	%	
ϕ_0^{s}	initial solid fraction	%	
$\phi_{\mathrm{s}}^{\mathrm{s}}$	initial solid fraction in the surrounding bone	%	
$\phi_{\mathrm{i}}^{\mathrm{s}}$	initial solid fraction at the implant	%	
ϕ^{f}	fluid fraction	%	
C^{c}	cell concentration	cell/mm^3	
C^{M}	growth factor concentration	ng/mm^3	
$q^{\mathrm{f/s}}$	fluid flow relative to the solid phase	mm/s	
$q^{\mathrm{c/s}}$	cell flow relative to the solid phase		
$q^{\mathrm{M/s}}$	growth factor flow relative to the solid phase		
Ω^{c}	cell phase source		
Ω^{s}	solid phase source		
Ω^{M}	growth factor source		
D^{c}	coefficient of cell diffusion		
D^{M}	coefficient of growth factor diffusion		
h^{c}	coefficient of haptotactic migration		
χ^{c}	coefficient of chemotactic migration		
α^{c}	coefficient of cell proliferation		
N^{cc}	Inhibition level of cell proliferation		
α^{s}	coefficient of osteoid synthesis		
r_{i}	radius of the implant surface	mm	
r_{s}	radius of the surrounding bone	mm	
r_{d}	radius of the drill hole	mm	
δ_{d}	transition path of solid fraction at the drill hole	mm	

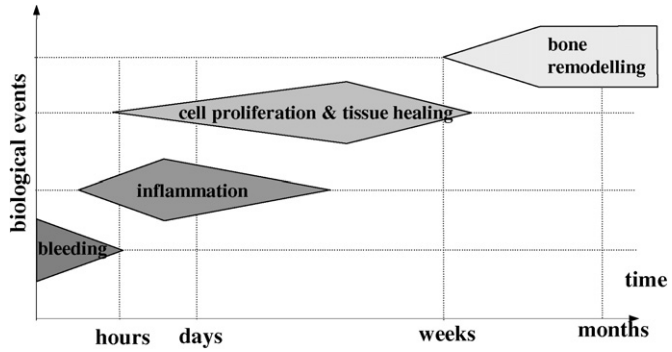

Fig. 1. Biological phases of tissue healing.

liferation, development, migration, differentiation and/or activity. It appears that they are of particular importance in the healing process since they largely govern the extra-cellular matrix fabrication (Alliston and Derynck, 2000; Conover, 2000). Blood vessels are growing (angiogenesis) in the healing site and allow cell metabolism to be viable. The mesenchymal cells differentiate into osteoblasts, which are cells responsible from the bone formation (Maheshwari and Lauffenburger, 1998). The following step is associated to the synthesis of bony mineral matrix and supported by the vascularization delivering calcium, phosphorus ions and growth factors (Dhert et al., 1988; Linkhart et al., 1996; Kibbin, 1997). The periprosthetic tissue healing is an intramembranous ossification and the synthesis of osteoid tissue into bone follows the formation of conjunctive fibrous tissue without an intermediary cartilaginous phase.

The mechanisms of cells migration are important when studying bone healing and remodelling and it particularly concerns the haptotactic and chemotactic active migrations (Puleo et al., 1991). Haptotaxis is the directed movement of cell motility or outgrowth either up or down a gradient of cellular adhesion sites. These gradients are naturally present in biological material. Chemotaxis is the phenomenon in which cells direct their movements according to certain chemicals in their environment (Friedl et al., 1998).

Experimental and clinical studies have shown the effects of implant coatings, interface motion, fluid pressure, and growth factors on implant fixation (Overgaard, 2000). Coupling with biological factors are also of prime influence to analyse the healing process (Søballe et al., 1992, 1993; Bechtold et al., 2001; Mouzin et al., 2001). The implant can be considered as a foreign body in the surrounding bone and it represents a strong perturbation from a mechano-biological point of view. The surgical technique, the use of bioactive coating, bone graft or additional growth factors are designed to improve the prosthesis fixation and generally to limit the heterogeneity of new-formed periprosthetic tissue unfavourable to the long term survival of the implant (Kold et al., 2005).

Predictive numerical models of the cells differentiation process and bone healing and remodelling have been developed using structural models and poroelastic approaches. The threshold of differentiation was predicted using a function of hydrostatic pressure and equivalent shear stress in structural models (Carter et al., 1988). More recent approaches involved shear strain and interstitial fluid velocity using poroelastic models (Prendergast, 1997). The biological phenomena and the time variable were not explicitly taken into account in these approaches. Relevant numerical models of migration and cellular differentiation taking into transient behaviour and biological factors were more recently developed (Tracqui, 1999; Bailon-Plaza and Van der Meulen, 2001). These studies provided significant progress in the numerical prediction of biological phenomena while simplifying mechanical aspects.

A reliable predictive model can assist in investigating the complicated phenomena of tissue healing and specially the heterogeneous healing. If associated to experimental validations it could help in improving implant design and surgical technique. We hypothesized that a fully mechano-biological model associating biological concept of cells migration to diffusion in porous media could help to predict the heterogeneity of osseous density in the early post-operative period. The study did not concern the initial inflammation, mesenchymal cells proliferation and differentiation but it focused on the bone formation by osteoblasts after differentiation. To proceed, a multiphasic model (solid, fluid, cell fractions and growth factors concentration) of porous tissue surrounding an unloaded axisymmetric implant was coupled to cell migration (convection, diffusion, haptotaxis, chemotaxis) and osseous matrix deposit (reactive medium). The numerical model was compared to experimental results from an ex-vivo histomorphometric study.

2. Description of the multiphasic model

2.1. Governing equations

As described in Fig. 2, the multiphasic model involved a solid phase ϕ^{s} relative to the extracellular osseous matrix, an extracellular fluid phase ϕ^{f} relative to the extracellular osseous marrow, a cellular part n^{c} relative to the osteoblasts population and a molecular part n^{M} relative to growth factors. The volume of growth factors considered as moles of ionic aqueous solutions and the volume of osteoblasts cells were supposed to be negligible compare to the fluid and solid volumes. The relationships between phases were expressed in term of elementary mass, Eq. (1), and volume fraction, Eq. (2).

$$m^{\mathrm{t}} = m^{\mathrm{s}} + m^{\mathrm{f}} = \rho^{\mathrm{s}} \cdot v^{\mathrm{s}} + \rho^{\mathrm{f}} \cdot v^{\mathrm{f}}, \tag{1}$$

$$\left(v^{\mathrm{s}} + v^{\mathrm{f}}\right)/v^{\mathrm{t}} = \phi^{\mathrm{s}} + \phi^{\mathrm{f}} = 1. \tag{2}$$

Concentrations C^{c} and C^{M}, were respectively defined in relations (3) and (4) using the density of cells N^{c} and the density of growth factors moles N^{M} in the connected pores of the tissue.

$$C^{\mathrm{c}} = N^{\mathrm{c}}/\left(v^{\mathrm{t}} - v^{\mathrm{s}}\right) = n^{\mathrm{c}}/\left(1 + \phi^{\mathrm{s}}\right), \tag{3}$$

$$C^{\mathrm{M}} = N^{\mathrm{M}}/\left(v^{\mathrm{t}} - v^{\mathrm{s}}\right) = n^{\mathrm{M}}/\left(1 + \phi^{\mathrm{s}}\right). \tag{4}$$

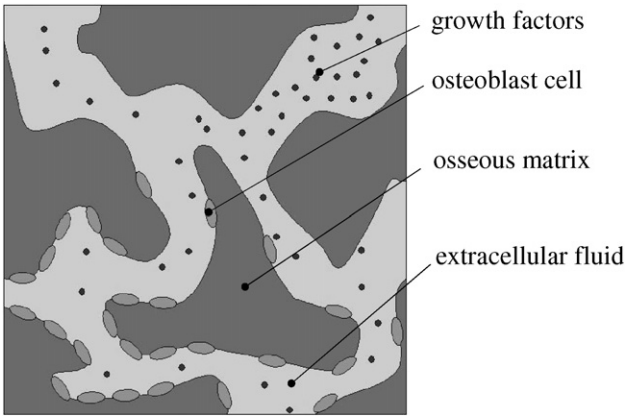

Fig. 2. Multiphasic model showing the architecture of porous medium involving the osseous or solid matrix, the extracellular fluid, the osteoblastic phase and the growth factor phase.

The laws of mass conservation of each phase were expressed by Eqs. (5)–(7) and (8). The osteoid source $\Omega_{\mathrm{m}}^{\mathrm{s}}$ was used in Eq. (5) to model the mineral deposit by osteoblasts during healing.

$$\frac{\partial}{\partial t}\left(\rho^{\mathrm{s}} \cdot \phi^{\mathrm{s}}\right) = \Omega_{\mathrm{m}}^{\mathrm{s}}. \tag{5}$$

Eq. (6) concerned the extracellular fluid conservation. The relative fluid flow $q^{\mathrm{f/s}}$ was used to model the fluid transfer which can induce transport of growth factors by convection.

$$\frac{\partial}{\partial t}\left(\rho^{\mathrm{f}} \cdot \phi^{\mathrm{f}}\right) = \sum_{i=1}^{3} \frac{\partial q_i^{\mathrm{f/s}}}{\partial x_i}. \tag{6}$$

The relative cells flow $q^{\mathrm{c/s}}$ was introduced in Eq. (7) to model the osteoblast cells migration. It was induced by diffusion and active haptotactic and chemotactic migrations. A mass source $\Omega_{\mathrm{m}}^{\mathrm{c}}$ was used to model the proliferation of cells.

$$\frac{\partial}{\partial t}\left(m^{\mathrm{c}} \cdot n^{\mathrm{c}}\right) = \sum_{i=1}^{3} \frac{\partial q_i^{\mathrm{c/s}}}{\partial x_i} + \Omega_{\mathrm{m}}^{\mathrm{c}}. \tag{7}$$

Concerning the growth factors conservation, the flow $q^{\mathrm{M/s}}$ was used in Eq. (8) to model exchanges by diffusion and convection. The formulation could permit to add a source of growth factors $\Omega_{\mathrm{m}}^{\mathrm{M}}$ (autologous or allologous growth factors).

$$\frac{\partial}{\partial t}\left(m^{\mathrm{M}} \cdot n^{\mathrm{M}}\right) = \sum_{i=1}^{3} \frac{\partial q_i^{\mathrm{M/s}}}{\partial x_i} + \Omega_{\mathrm{m}}^{\mathrm{M}}. \tag{8}$$

The cellular migration expressed by Eq. (9) associated the diffusion D^{c} (Dee et al., 1999) and the mechanisms of migration by haptotaxis (h^{c}) and by chemotaxis (χ^{c}). Haptotactic flow was proportional to the solid fraction gradient and chemotactic flow was proportional to the growth factors gradient (Friedl et al., 1998).

$$q_i^{\mathrm{c/s}} = m^{\mathrm{c}}\left(1 - \phi^{\mathrm{s}}\right)\left[D^{\mathrm{c}} \frac{\partial C^{\mathrm{c}}}{\partial x_i} - h^{\mathrm{c}} C^{\mathrm{c}} \frac{\partial\left(\rho^{\mathrm{s}} \phi^{\mathrm{s}}\right)}{\partial x_i} - \chi^{\mathrm{c}} C^{\mathrm{c}} \frac{\partial C^{\mathrm{M}}}{\partial x_i}\right]. \tag{9}$$

The flow of growth factors expressed by Eq. (10) was diffusive (D^{M}) and convective.

$$q_i^{\mathrm{M/s}} = m^{\mathrm{M}}\left[D^{\mathrm{M}} \phi^{\mathrm{f}} \frac{\partial C^{\mathrm{M}}}{\partial x_i} + C^{\mathrm{M}} q_{\mathrm{v}}^{\mathrm{f/s}}\right]. \tag{10}$$

Table 1
Boundary conditions of the model

Parameter	Location	
	r_i: implant surface	r_s: surrounding bone
q^f (mm/s)	0	–
q^c (cell/mm^2 s)	0	–
q^M (ng/mm^2 s)	0	–
n^c (cell/mm^3) (Bailon-Plaza and Van der Meulen, 2001)	–	1000
n^M (ng/mm^3)	–	0

It was assumed that each phase was incompressible ($\partial\rho/\partial t = 0$). Eq. (7) was completed using the volume source of cells Ω_v^c derived from the logistic law (11), involving a coefficient of proliferation speed α^c and the limit of proliferation N^{cc} (Tranqui and Tracqui, 2000).

$$\Omega_v^c = \alpha^c n^c \left(N^{cc} - n^c\right). \tag{11}$$

It is biologically observed that the osteoid secretion from the osteoblastic population is promoted by growth factors (Linkhart et al., 1996). In that case, the multiphasic medium could be considered as reactive medium described by Eq. (12) where the solid matrix source was proportional to the growth factors density n^M.

$$\Omega_v^s = \alpha^s n^c n^M. \tag{12}$$

Eqs. (5)–(8), modified using the behavior laws (9)–(12) led to the highly coupled convective-diffusive set of Eqs. (13)–(16). Output measures were the solid fraction ϕ^s, the relative fluid flow $q^{f/s}$, the cellular concentration of osteoblasts C^c and the concentration of growth factors C^M.

$$\frac{\partial \phi^s}{\partial t} = \alpha^s \left(1-\phi^s\right)^2 C^c C^M, \tag{13}$$

$$\sum_{i=1}^{3} \frac{\partial q_i^{f/s}}{\partial x_i} + \frac{\partial \phi^s}{\partial t} = 0, \tag{14}$$

$$\begin{aligned}
&\left(1-\phi^s\right)\frac{\partial C^c}{\partial t} + \left[\left(D^c + h^c\rho^s\left(1-\phi^s\right)\right)\frac{\partial \phi^s}{\partial x_i} + \chi^c\left(1-\phi^s\right)\frac{\partial C^M}{\partial x_i}\right]\frac{\partial C^c}{\partial x_i} \\
&\quad = \left(1-\phi^s\right)D^c\frac{\partial^2 C^c}{\partial x_i^2} + h^c\rho^s C^c\left[\left(\frac{\partial \phi^s}{\partial x_i}\right)^2 - \left(1-\phi^s\right)\frac{\partial^2 \phi^s}{\partial x_i^2}\right] + \chi^2 C^c\left[\frac{\partial \phi^s}{\partial x_i}\frac{\partial C^M}{\partial x_i} - \left(1-\phi^s\right)\frac{\partial^2 C^M}{\partial x_i^2}\right] \\
&\qquad + \alpha^c\left(1-\phi^s\right)C^c\left(N^{cc} - \left(1-\phi^s\right)C^c\right) + C^c\frac{\partial \phi^s}{\partial t},
\end{aligned} \tag{15}$$

$$\left(1-\phi^s\right)\frac{\partial C^M}{\partial t} + \left(D^M\frac{\partial \phi^s}{\partial x_i} - q_i^{f/s}\right)\frac{\partial C^M}{\partial x_i} = D^M\left(1-\phi^s\right)\frac{\partial^2 C^M}{\partial x_i^2}. \tag{16}$$

2.2. Numerical model of the canine implant

The previous general formulation was reduced to the axisymmetric model (radius r, time t) of the canine implant (Søballe et al., 1992; Vestermark et al., 2004) shown in Figs. 3(a) and 3(b). The computation of ϕ^s, $q^{f/s}$, C^c and C^M was achieved using a first order finite differences scheme in time and a second order scheme in space (0.02 mm). The Newton–Raphson algorithm was used to solve non-linearities due to couplings (Ames-William, 1977). The healing process was evaluated up to 8 weeks after the implantation, which was in good agreement with in-vivo observation, so the computation time was optimized using a variable time step. The model was implemented into the Matlab® environment (The Mathworks Company).

As described in Table 1, the boundary conditions concerning fluid flow, cells flow and growth factors flow were nil at the implant surface. It was assumed a specific cellular concentration and a nil growth factor concentration in the surrounding bone. The initial conditions are described in Table 2. Growth factors were present in the implant

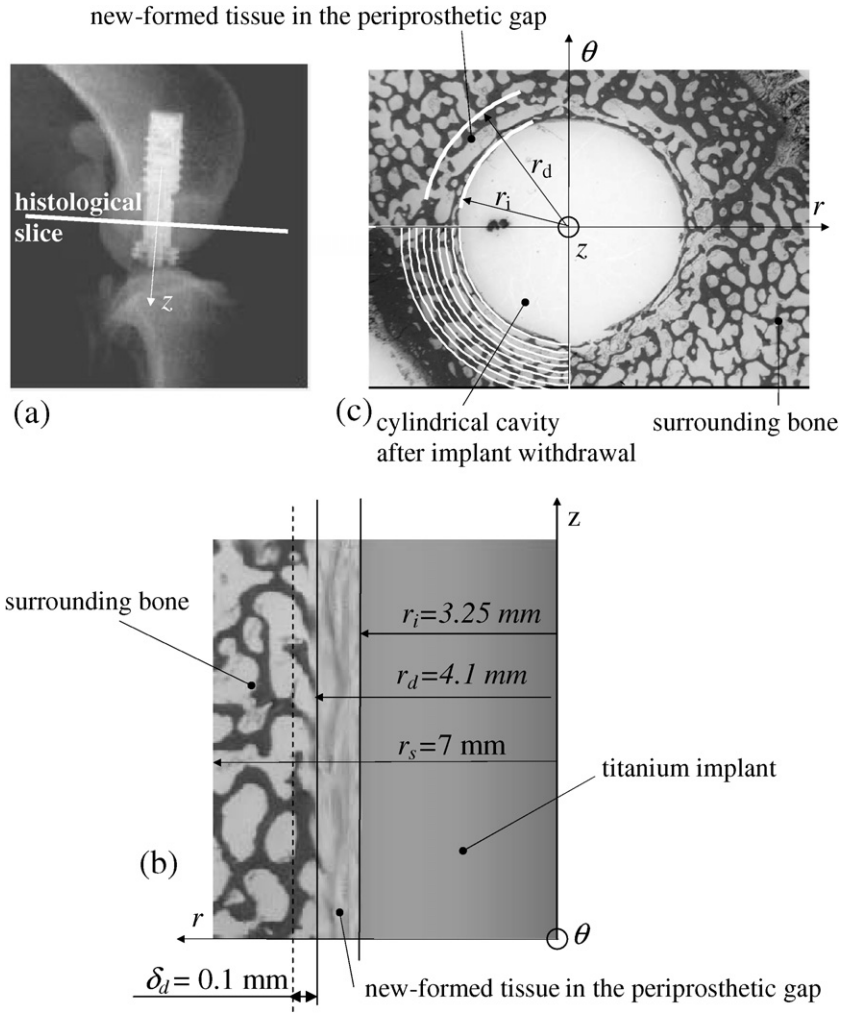

Fig. 3. Canine implant (Søballe et al., 1992): (a) in-vivo implantation (x-ray), (b) axisymmetric model, (c) histological slice showing the biological tissue distribution.

Table 2
Initial conditions of the model

Parameter	Location	
	$[r_i, r_d]$: new-formed tissue	$[r_d, r_s]$: surrounding bone
ϕ^s (%)	0.06	0.1–0.6
q^f (mm/s)	0	0
n^c (cell/mm^3) (Bailon-Plaza and Van der Meulen, 2001)	[0;1000]	1000
C^M (ng/mm^3) (Bailon-Plaza and Van der Meulen, 2001)	[0;0.3]	0

surrounding gap to stimulate the tissue healing and the recruitment of osteoblasts towards the healing site. The supplementary source of growth factors, Ω_m^M in Eq. (8), was supposed to be nil. The initial heterogeneity of the solid fraction ϕ_0^s was rather high and it was modelled by the continuous equation (17), involving the initial solid fractions ϕ_i^s and ϕ_s^s. The geometrical parameters δ_d and r_d shown in Fig. 3(b), were dependent from the surgical technique.

$$\phi_0^s = \frac{1}{2}\left(\phi_s^s + \phi_i^s\right) + \frac{1}{\pi}\left(\phi_s^s - \phi_i^s\right)\tan^{-1}\left[\frac{1}{\delta_d}(r - r_d)\right]. \tag{17}$$

Table 3
Invariable data of the model

Parameter		Value
r_i (mm)	(Vestermark et al., 2004)	3.25
r_s (mm)	(Vestermark et al., 2004)	7
r_d (mm)	(Vestermark et al., 2004)	4.1
δ_d (mm)	(Vestermark et al., 2004)	0.1
N^{cc} (cell/mm^3)	(Bailon-Plaza and Van der Meulen, 2001)	1000
α^c (mm^3/cell s)	(Tranqui and Tracqui, 2000)	1.9×10^{-10}
D^c (mm^2/s)	(Dee et al., 1999)	2.5×10^{-7}
D^M (mm^2/s)	(Maheshwari and Lauffenburger, 1998)	4.8×10^{-6}
ρ^s (kg/mm^3)	Fung (1981)	2.57×10^{-6}

Table 4
Variable data of the model

Parameter		Value
ϕ_s^s (%)		[10; 60]
C^M (ng/mm^3)	(Bailon-Plaza and Van der Meulen, 2001)	[0.; 0.3]
α^s (mm^6/cell ng s)	(Bailon-Plaza and Van der Meulen, 2001)	$[1 \times 10^{-9}; 5 \times 10^{-9}]$
n^c (cell/mm^3)	(Bailon-Plaza and Van der Meulen, 2001)	[0.; 1000]
h^c (mm^5/s kg)	(Friedl et al., 1998)	[0.04; 1.25]
χ^c (mm^5/s ng)	(Maheshwari and Lauffenburger, 1998)	$[1 \times 10^{-5}; 32.5 \times 10^{-5}]$

2.3. Experimental data from the ex-vivo histological study:

At euthanasia, the knees were surgically exposed and the distal femur was removed and frozen at $-20\,^\circ$ C. One piece was cut perpendicular to the implant using a water-cooled diamond band. It was used to prepare ground sections for identification of patterns of bone distribution in the former gap and surrounding bone. The specimen were fixed in 70% ethanol, dehydrated in graded ethanol (70–90%), embedded in methylmethacrylate, and ground and polished (Exact-Micro Grinding System) to approximately 20 microns thickness. They were stained with 0.4% basic fuchsin, and counterstained with 2% light green for 6 minutes. This process permitted to display the osseous or mineralized tissue in dark grey and the fibrous tissue in white (Vestermark et al., 2004).

As described previously, the solid fraction ϕ^s (osseous or mineral fraction) was one of the output measure the numerical model. To achieve the numerical-experimental comparison, the numerical image of the histological cut required a specific post-treatment. As shown in Fig. 3(c), the domain was divided into concentric zones where the osseous fraction was computed as the ratio of osseous pixels sum (dark grey) over the overall pixels sum. For clarity, only a quarter is plotted in Fig. 3(c). The space step of both the numerical model and the experimental data were 0.02 mm and the overall value of the osseous fraction distribution was computed from five histological slices of the same implant.

2.4. Updating of the numerical model

The numerous parameters of the numerical model did not involve the same reliability level. Referring to the literature and clinical experience, it was chosen to sort them into two main groups. Table 3 describes eight constant data of the model. The geometry of the implant (r_i, r_s) and the clinical gesture (r_d, δ_d) was reasonably well controlled. Biological coefficients (N^{cc}, α^c, D^c, D^M, ρ^s) did not show the largest discrepancies in the literature. Six biological parameters were varying in the range presented in Table 4. Despite a few data in the literature it was difficult to obtain robust coefficients relative to the behaviour of the osteoblastic phase. (C^M, α^s, n^c) and in particular the active migration properties (h^c, χ^c). Starting from a set of mean value, the parameters were successively updated until obtaining a satisfying correlation with the periprosthetic osseous (or mineral) distribution derived from the ex-vivo histological results.

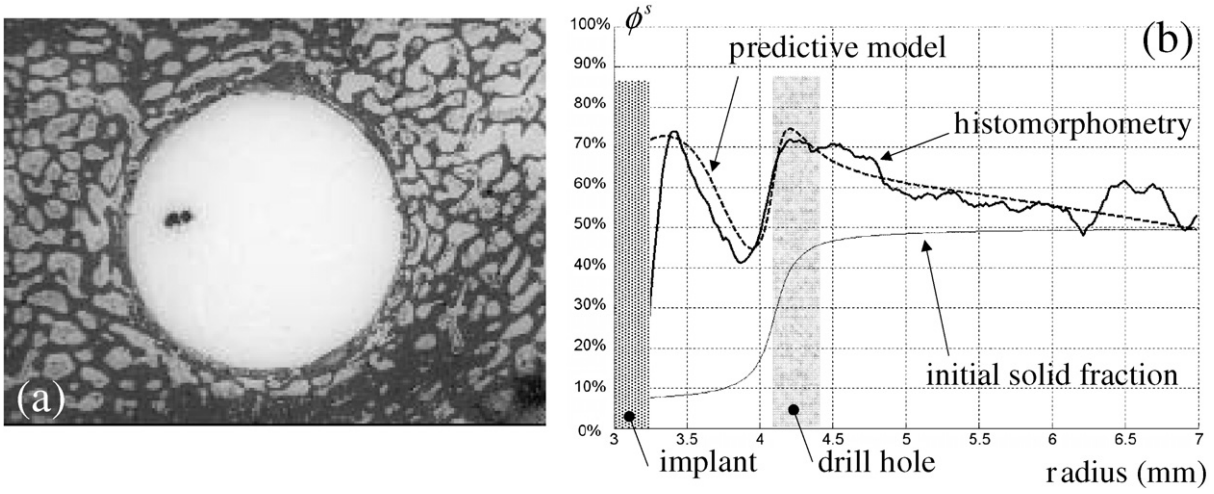

Fig. 4. Homogeneous healing with high bone formation: (a) ex-vivo result from histomorphometry, (b) osseous (solid) fraction distribution ϕ^{s} (%).

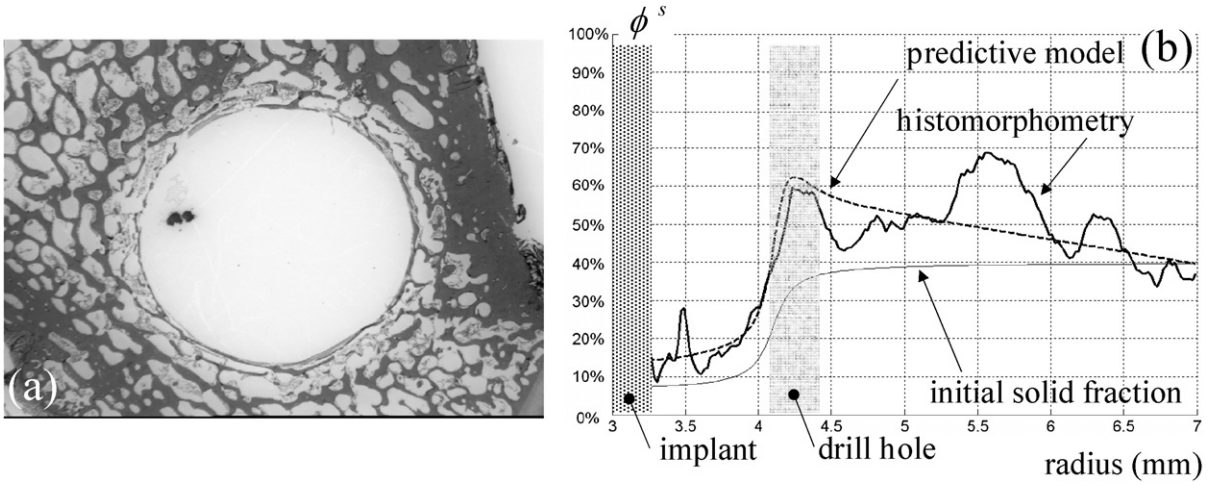

Fig. 5. Homogeneous healing with low bone formation: (a) ex-vivo result from histomorphometry, (b) osseous (solid) fraction distribution ϕ^{s} (%).

3. Results

As shown in Figs. 4, 5 and 6, the distribution of the osseous or mineral tissue (ϕ^{s}) showed two main oscillations in the radial direction. Criteria based upon magnitude and locations of peaks allowed the periprosthetic healing to be sorted into three main categories: homogeneous healing with high ossification, healing with low ossification, heterogeneous healing with a peak of high ossification.

3.1. Homogeneous healing with high bone formation

The predicted and experimental results are shown in Fig. 4. The osseous fraction ϕ^{s} was in the range $58\% \pm 30\%$ which was a rather high magnitude relative to a very satisfying healing. Initial cell and growth factor concentrations (Table 2) were homogeneous and the numerical values used to update the model were as follows:

$$\phi_{\mathrm{s}}^{\mathrm{s}} = 50\%; \quad \alpha^{\mathrm{s}} = 3 \times 10^{-9}\ \mathrm{mm}^6/\mathrm{s\,cell\,ng}; \quad h^{\mathrm{c}} = 0.7\ \mathrm{mm}^5/\mathrm{s\,kg},$$
$$\chi^{\mathrm{c}} = 3 \times 10^{-5}\ \mathrm{mm}^5/\mathrm{s\,ng}; \quad C^{\mathrm{M}} = 0.2\ \mathrm{ng/mm}^3; \quad n^{\mathrm{c}} = 1000\ \mathrm{cell/mm}^3.$$

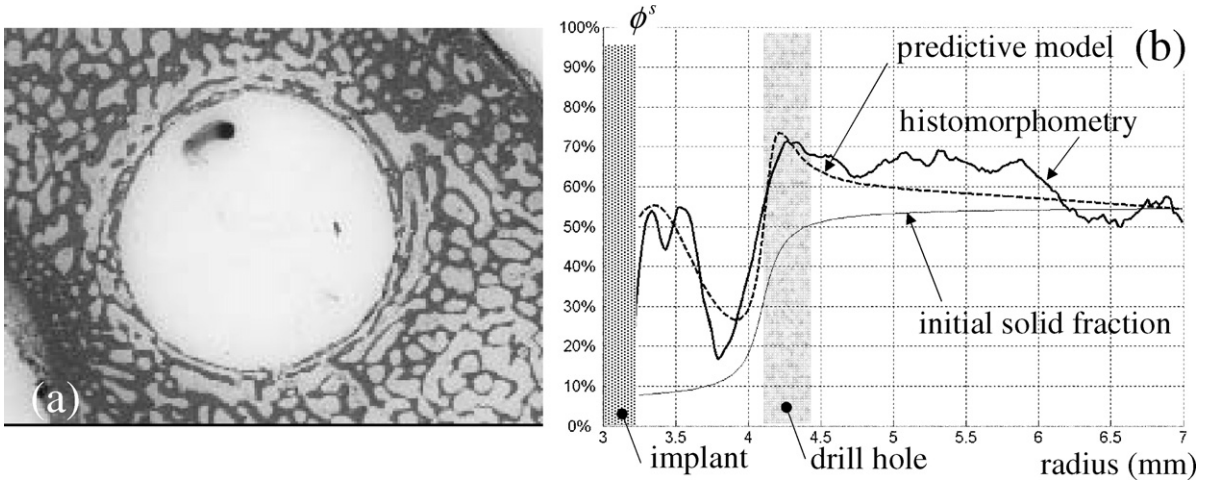

Fig. 6. Heterogeneous healing with a peak of high bone formation: (a) ex-vivo result from histomorphometry, (b) osseous (solid) fraction distribution ϕ^{s} (%).

3.2. Homogeneous healing with low bone formation

The predicted and experimental results are shown in Fig. 5. A very poor healing was obtained. The solid fraction ϕ^{s} remained about 60% at the drilling hole, but a fast and continuous decrease appeared toward the implant surface Fibrous tissue appeared into the periprosthetic gap (available space between the implant surface and the drill hole) with a mean value of 25% for ϕ^{s}. The initial growth factor concentration was homogeneous (Table 2) both in the gap and the surrounding bone, but it was necessary to modify the homogeneous initial cells distribution to fit with the histological results. The osteoblast phase was initially located at the drill hole: the cell concentration n^{c} was 1000 cell/mm^3 in the surrounding bone and nil into the gap. Finally, the updated values of the numerical model were as follows:

$$\phi^{\mathrm{s}}_{\mathrm{s}} = 40\%; \quad \alpha^{\mathrm{s}} = 3.5 \times 10^{-9}\ \mathrm{mm}^6/\mathrm{s\,cell\,ng}; \quad h^{\mathrm{c}} = 0.78\ \mathrm{mm}^5/\mathrm{s\,kg},$$
$$\chi^{\mathrm{c}} = 5 \times 10^{-5}\ \mathrm{mm}^5/\mathrm{s\,ng}; \quad C^{\mathrm{M}} = 0.2\ \mathrm{ng/mm}^3; \quad n^{\mathrm{c}} = 0\ \mathrm{cell/mm}^3.$$

3.3. Heterogeneous healing with a peak of high bone formation

The predicted and experimental results are shown in Fig. 6. The osseous fraction ϕ^{s} was in the range $47\% \pm 62\%$. This healing showed rather large discrepancies of solid fraction in the radial direction. Furthermore a peak of mineralized tissue ($\phi^{\mathrm{s}} \approx 55\%$) was predicted in the gap at a average distance of 0.25 mm from the implant. This osseous rim showed an average thickness of 0.2 mm and it was connected to the surrounding bone (drill hole) by fibrous tissue ($\phi^{\mathrm{s}} \approx 20\%$). From a biological point of view, this neo-formed tissue could be similar to sclerotic bone rim generally before revision of human prosthesis. The updated values of the numerical model were as follows:

$$\phi^{\mathrm{s}}_{\mathrm{s}} = 55\%; \quad \alpha^{\mathrm{s}} = 1.4 \times 10^{-9}\ \mathrm{mm}^6/\mathrm{s\,cell\,ng}; \quad h^{\mathrm{c}} = 1\ \mathrm{mm}^5/\mathrm{s\,kg},$$
$$\chi^{\mathrm{c}} = 4 \times 10^{-5}\ \mathrm{mm}^5/\mathrm{s\,ng}; \quad C^{\mathrm{M}} = 0.2\ \mathrm{ng/mm}^3; \quad n^{\mathrm{c}} = 1000\ \mathrm{cell/mm}^3.$$

4. Discussion & conclusion

The periprosthetic tissue healing is an intramembranous ossification and the synthesis of osteoid tissue into bone follows the formation of conjunctive fibrous tissue without an intermediary cartilaginous phase. Our approach was in agreement with this physiological consideration. A general formulation of governing equations of porous media coupled with biological equations was proposed and applied in a second step to predict the healing of an axisymmetric canine implant. Although the complexity of mechano-biological phenomena was high, the comparison of predicted and histomorphometric results showed a satisfying agreement. So, it appeared that our hypothesis coupling biological

concept of cells migration to diffusion (active and passive) in porous media was reliable at least at the first order. In our knowledge, the proposed model was the first spatial-temporal model allowing such implant healing to be numerically predicted.

This study highlighted how a theoretical model could help in the investigation of mechano-biological phenomena but it is well known that the robustness of a predictive model is always dependent upon the reliability of input data, boundary and initial conditions, and in our non-linear model, this aspect was particularly prominent. One way to evaluate the limitation of our assumptions was to implement a mixed numerical-experimental approach.

A significant assumption was that both the numerical model and the experimental canine implant involved axisymmetrical properties and mechano-biological behaviour. The clinical parameters such as the implant radius r_i and the drill hole radius r_d were reasonably controlled but involved axial positioning and circularity coupled default ($\pm 5\%$). The post-treatment method of the ex-vivo histological slices based on pixel counting in perfect concentric zone was sensitive to these geometrical defaults. The discrepancies between numerical and experimental results were also partly due to the local alteration of the interface at the inner surface (r_i) during the implant withdrawal.

On the other hand, biological factor such as cell and growth factor concentrations, cell active migration coefficients, involved the most significant uncertainties. So an empirical update procedure was implemented starting from mean values of the literature (see Table 4) to obtain the three main pattern of osseous distribution observed in-vivo (Figs. 4–6). Finally, the results were satisfying and it appeared that the process converged toward final values in the range of variation described in the literature.

At the beginning of the healing process, the domain surrounding the implant was highly heterogeneous: the porosity of the surrounding bone was kept intact although the porosity into the gap was very low because highly modified by the surgical gesture. The porosity step was located at the drill hole (radius r_d). It could be initially assumed that the tissue heterogeneity induced a significant influence on the osteoblast cells and growth factors diffusion and the satisfying numerical–experimental comparison confirmed this hypothesis. It also appeared that the distribution of the initial solid fraction by the continuous inverse tangent function (Eq. (17)) had an effect on the radial shifts between the predicted and experimental results; this influenced the haptotactic active migration.

The bone formation into the periprosthetic tissue was highly sensitive to the osteoblast concentration. As shown in Fig. 1, the initial distribution of cells came from the transient phases preceding the healing process: inflammation and differentiation. The model involved two active cellular mechanisms described as haptotactic and chemotactic migrations which interactions with the solid fraction and the growth factor concentration was depending on the healing history. In the studied implant, the chemotactic migration made the osteoblasts to move towards the implant surface because of the presence of highest growth factor gradients of same algebraic sign during the healing process. On the opposite, the haptotactic migration tended to concentrate the cells at the drill hole (r_d) where the highest gradient of solid fraction appeared. These conflicting phenomena induced the reduction of the osteoblasts number into the periprosthetic gap, so the privileged locations for bone formation were close from the implant surface and at the drill hole. The growth of bone tissue in these last zones while locally reducing the tissue porosity amplified the phenomenon by decreasing the possibilities of balanced access of new cells within the bone–implant interface. This analysis could explain the two main oscillations of the osseous fraction distributions shown in Figs. 4 to 6. Heterogeneous bone formation and specially the formation of a condensed or sclerotic bone rim into the periprosthetic gap were increased for higher values of haptotactic coefficient (h^c). This was unfavourable to the long term survival of the implant.

In our formulation, the governing equations have been written in the case of no mechanical strain appeared into the phases. The ex-vivo histological data from the canine axisymmetric were valid in the same framework. Histological data from unstable and loaded implants generally showed a significant influence of the mechanical stimuli and specially the emphasis of heterogeneous bone healing. The extension of the mechano-biological formulation to deformable reactive porous media and a finite element resolution are currently implemented. For both stable and unstable implant the judicious use of experimental design procedure will also help to rank the role of mechano-biological parameters.

Further mixed numerical-experimental investigations to quantify biological parameters could be pertinent. It is envisaged to design specific mechano-biological experiments with cell cultures (osteoblast cell) to evaluate active migration behaviour controlling growth factor concentration and/or porosity gradient of the substrate. Inverse method based on 2D poroelastic models could be used to identify unknown parameters. But contrarily to fully controlled and manufactured inert mechanisms, the prediction of the mechanical behaviour of biological media would involve incontrovertible uncertainties and variability.

Using our approach to improve the long term survival of human implant cold be envisaged after supplementary validations. The clinical aim is to favour the homogeneous bone formation to limit and if possible, avoid the revision of human prosthesis. The model could assist in evaluating the role of growth factor concentrations and their temporal delivering as far as the role of pertinent sources such as bioactive coating or additional biomaterials.

Acknowledgements

This work was completed thanks to J.E. Bechtold PhD (Midwest Orthopaedic Research Foundation) and K. Søballe MD, PhD (University Hospital of Aarhus, Denmark) who associated the authors to their research activity in implant fixation. We also thank M. Vestermark-Toft and F. Melsen (University Hospital of Aarhus, Denmark) for the ex-vivo histomorphometric data.

References

Alliston, T.N., Derynck, R., 2000. Transforming growth factor β in skeletal development and maintenance. In: Canalis, E. (Ed.), Skeletal Growth Factors. TPA, Philadelphia, pp. 233–249.

Ames-William, F., 1977. Numerical Methods for Partial Differential Equations, second ed. Computer Science and Applied Mathematics. Academic Press, New York.

Bailon-Plaza, A., Van der Meulen, M.C., 2001. A mathematical framework to study the effects of growth factor influences on fracture healing. J. Theor. Biol. 212 (2), 191–209.

Bechtold, J.E., Mouzin, O., Kidder, L., Søballe, K., 2001. A controlled experimental model of revision implants: Part II. Implementation with loaded titanium implants and bone graft. Acta Orthop. Scand. 72 (6), 650–656.

Carter, D.R., Blenman, P.R., Beaupre, G.S., 1988. Correlations between mechanical stress history and tissue differentiation in initial fracture healing. J. Orthop. Res. 6 (5), 736–748.

Conover, C.A., 2000. Insulin-like Growth Factors and the skeleton. In: Canalis, E. (Ed.), Skeletal Growth Factors. TPA, Philadelphia, pp. 101–116.

Dee, K.C., Anderson, T.T., Bizios, R., 1999. Osteoblast population migration characteristics on substrates modified with immobilized adhesive peptides. Biomaterials 20 (3), 221–227.

Dhert, W.J., Thomsen, P., Blomgren, A.K., Esposito, M., Ericson, L.E., Verbout, A.J., 1988. Integration of press-fit implants in cortical bone: a study on interface kinetics. J. Biomed. Mater. Res. 41 (4), 574–583.

Friedl, P., Zanker, K.S., Brocker, E.B., 1998. Cell migration strategies in 3-D extracellular matrix: differences in morphology, cell matrix interactions, and integrin function. Microsc. Res. Tech. 43 (5), 369–378.

Fung, Y.C., 1981. Biomechanical Properties of Living Tissues. Springer-Verlag, New York.

Hahn, M., Vogel, M., Eckstein, F., Pompesius-Kempa, M., Delling, G., 1998. Bone structure changes in hip joint endoprosthesis implantation over the course of many years. A quantitative study. Chirurg. 59 (11), 782–787.

Kibbin, M.B., 1997. The biology of fracture healing in long bones. J. Bone Joint Surg. Am. 79, 1938–1941.

Kold, S., Bechtold, J.E., Mouzin, O., Elmengaard, B., Chen, X., Søballe, K., 2005. Fixation of revision implants is improved by a surgical technique to crack the sclerotic bone rim. Clin. Orthop. Relat. Res. 432, 160–166.

Linkhart, T.A., Mohan, S., Baylink, D.J., 1996. Growth factors for bone growth and repair: IGF, TGF beta and BMP. Bone 19 (Suppl. 1), 1S–12S (Review).

Maheshwari, G., Lauffenburger, D.A., 1998. Deconstructing (and reconstructing) cell migration. Microsc. Res. Tech. 43 (5), 358–368.

Mouzin, O., Søballe, K., Bechtold, J.E., 2001. Loading improves anchorage of hydroxyapatite implants more than titanium implants. J. Biomed. Mater. Res. 58 (1), 61–68.

Overgaard, S., 2000. Calcium phosphate coatings for fixation of bone implants. Acta Orthop. Scand. 71 (Suppl. 297).

Prendergast, P.J., 1997. Finite element models in tissue mechanics and orthopaedic implant design. Clin. Biomech. (Bristol, Avon) 12 (6), 343–366.

Puleo, D.A., Holleran, L.A., Doremus, R.H., Bizios, R., 1991. Osteoblast responses to orthopedic implant materials in vitro. J. Biomed. Mater. Res. 25 (6), 711–723.

Søballe, K., Hansen, E.S., B-Rasmussen, H., Jorgensen, P.H., Bunger, C., 1992. Tissue ingrowth into titanium and hydroxyapatite-coated implants during stable and unstable mechanical conditions. J. Orthop. Res. Mar. 10 (2), 285–299.

Søballe, K., Toksvig-Larsen, S., Gelineck, J., Fruensgaard, S., Hansen, E.S., Ryd, L., Lucht, U., Bunger, C., 1993. Migration of hydroxyapatite coated femoral prostheses. A Roentgen Stereophotogrammetric study. J. Bone. Joint Surg. Br. 75 (5), 681–687.

Vestermark, M.T., Bechtold, J.E., Swider, P., Søballe, K., 2004. Mechanical interface conditions affect morphology and cellular activity of sclerotic bone rims forming around experimental loaded implants. J. Orthop. Res. 22 (3), 647–652.

Tracqui, P., 1999. Modèles continus de populations cellulaires en migration. In: Ronot, X., Schoëvaërt-Brossault, D. (Eds.), Dynamique de la cellule vivante. Inserm, pp. 195–222.

Tranqui, L., Tracqui, P., 2000. Mechanical signalling and angiogenesis. The integration of cell-extracellular matrix couplings. C. R. Acad. Sci. Ser. III 323 (1), 31–47.